First Principles Study of Electronic and Magnetic Properties of $Gd_{1-x}Ho_xMnO_3$

Zhu Xingfeng, Wang Yaxu

(School of Physics and Technology, Nanjing Normal University, Nanjing 210046, China)

Abstract: Using first-principles density functional theory within the generalized gradient approximation method, the effect of electronic and magnetic properties of a series of orthorhombic manganites $Gd_{1-x}Ho_xMnO_3$ ($0.0 \leqslant x \leqslant 0.5$) have been studied. For all concentrations we find that the single orthorhombic structure in $Gd_{1-x}Ho_xMnO_3$ can be maintained and the volume of the unit cell can almost be linear decreasing with x. It is found that the Mn – O – Mn bond angle decreases almost linearly with the Ho doping which originates the enhanced electric polarization in $Gd_{1-x}Ho_xMnO_3$. The AFM-E phase becomes more stable due to the Ho doping and the local magnetic moment of Mn is basically constant for all x in $Gd_{1-x}Ho_xMnO_3$ based on the magnetic properties calculations.

Key words: multiferroic, first-principles, electronic structure, magnetic properties

CLC number: O469 **Document code:** A **Article ID:** 1001-4616(2012)02-0039-06

第一性原理研究 $Gd_{1-x}Ho_xMnO_3$ 的电子结构和磁学性质

朱兴凤,王亚戍

(南京师范大学物理科学与技术学院,江苏 南京 210046)

[摘要] 利用第一性原理方法研究了一系列正交结构锰酸盐 $Gd_{1-x}Ho_xMnO_3$ ($0.0 \leqslant x \leqslant 0.5$) 的电子结构和磁学性质. 我们研究的所有组分的 $Gd_{1-x}Ho_xMnO_3$ 都能保持单一的立方结构,单胞的体积也随着 x 的增大线性减小,Mn – O – Mn 键的键角也随着 Ho 的掺杂而线性的减小. 我们的磁属性研究表明随着 Ho 的掺杂反铁磁 – E 相变越来越稳定,Mn 的磁矩随着 x 的增大基本不变.

[关键词] 多铁,第一性原理,电子结构,磁属性

Multiferroic oxides have attracted considerable recent attention due to their intriguing coupling between the magnetic and electric order parameters [1-5]. Of all the known multiferroic materials, the $RMnO_3$ rare-earth manganites attracted particular interest. The rare-earth manganites prepared under ordinary synthetic conditions crystallize in the orthorhombic perovskite structure (o-$RMnO_3$) for R = La-Dy with large ionic radius and in the hexagonal structure (h-$RMnO_3$) for R = Ho-Lu with smaller ionic radius. However, by means of special soft-chemistry synthesis, applying pressure, or even epitaxial thin-film growth, the hexagonal structure can be converted into the more dense, albeit metastable orthorhombic phase [6-8] and the o-$RMnO_3$ manganites show a rich variety of subtle interplay among charge, spin, orbital, and lattice degrees of freedom [4,5].

Received date: 2011-12-09.

Foundation item: Supported by the Natural Science Foundation of China(11147185) and the Natural Science Foundation of the Jiangsu Higher Education Institutions of China (10KJB140005). Numerical calculation was carried out using the facilities of the Department of Physics in Nanjing Normal University.

Corresponding author: Zhu Xingfeng, lecturer, majored in condensed material physics. E-mail: zhuxingfeng@njnu.edu.cn

Notably, a special antiferromagnetic (AFM) phase has been observed in o-$RMnO_3$ with the zigzag chains of ferromagnetic (FM) spins, antiferromagnetically coupled to neighboring chains or the E-type in the Wollan-Koehler standard notation. It is somewhat surprising that the E-type phase was predicted to be stable over a wide region of the phase space [9,10]. Moreover, both theoretical and experimental works demonstrate the existence of spontaneous polarization triggered by such a magnetic configuration with broken spatial inversion symmetry [11,12]. The most significant effect on the orthorhombic structure by decreasing ionic radius is to enhance the cooperative rotation of the MnO_6 octahedra. The resulting substantial bending of the Mn - O - Mn angle will weaken the FM superexchange interactions between nearest-neighbor Mn ions due to a reduction in the overlap of Mn and O orbitals. Therefore, the AFM interactions between Mn ions from different zigzag chains through the Mn - O - O - Mn or the Mn - O - Mn path would need to be taken into account and the APM-E type state becomes stable. A simple strategy is to reduce the R-site ionic size by substituting the R-site ions with small rareearth ions such as Ho, Y, Tm etc, so that the Mn - O - Mn bond angle can be reduced to favor the AFM-E order. Along the roadmap mentioned above, one can choose $GdMnO_3$ as a prototype and perform the Ho-doping at the Gd site, noting that $GdMnO_3$ exhibits the AFM-A order but close to the boundary with the noncollinear spiral spin (NSS) order [13,14].

To understand the physics involved in these multiferroic materials, it is necessary to understand their electronic structure and magnetic properties. Compared to o-$RMnO_3$, the detailed electronic structure and magnetic properties of $Gd_{1-x}Ho_xMnO_3$ are not very well understood. In this paper we study the effect of Ho doping on the electronic structure and magnetic properties in order to shed light on the questions raised by the experimental studies.

1 Computational Details

Experimentally, the unit cell in orthorhombic $GdMnO_3$ shows the *Pnma* symmetry (whereas the *Pnma* setting is used in some other references, the standard *Pnma* orientation is adopted in this paper, i.e., we choose *b* as the longest axis), with strong distortions with respect to the ideal cubic perovskite. To study the electronic and magnetic properties of $Gd_{1-x}Ho_xMnO_3$ ($0.0 \leqslant x \leqslant 0.5$), we have constructed a supercell consisting of 40 atoms. We consider substitute forms in our initial configuration as follows: for $x = 0.125$, we replace one Gd atom with Ho at (0.20, 0.25, 0.02); for $x = 0.25$, we replace two Gd atoms with Ho at (0.20, 0.25, 0.02) and (0.71, 0.25, 0.02); for $x = 0.375$, we replace three Gd atoms with Ho at (0.20, 0.25, 0.02), (0.71, 0.25, 0.02) and (0.54, 0.75, 0.52); for $x = 0.5$, we replace four Gd atoms with Ho at (0.20, 0.25, 0.02), (0.71, 0.25, 0.02), (0.45, 0.25, 0.48) and (0.95, 0.25, 0.48). We have considered four kinds of AFM spin configurations: AFM-A, AFM-C, AFM-G and AFM-E in 40 atoms/unit cell. We recall that, according to the standard Wollan-Koehler notation, the AFM-A shows ferromagnetic (FM) (AFM) intraplanar (interplanar) coupling; the AFM-C shows FM (AFM) interplanar (intraplanar) coupling; the AFM-G shows AFM in both intra-and interplanar coupling. The AFM-E shows in-plane FM zigzag chains antiferromagnetically coupled to the neighboring chains. The reason why we used the AFM-A and AFM-E configuration in Ho doping systems is based on the fact that the $GdMnO_3$ and $HoMnO_3$ show as ground state the AFM-A and AFM-E spin configuration respectively.

We perform simulations based on the Perdew-Burke-Ernzerhof (PBE) [16] version of the generalized gradient approximation (GGA) to density-functional theory (DFT) using the Vienna Ab initio Simulation Package (VASP) [17] and the projectoraugmented-wave (PAW) pseudopotentials. The number of plane waves in VASP is controlled by the cut-off energy, which in all our static calculations is 400 eV, while all the geometry relaxations are performed with an increased cut-off of 500 eV to ensure proper convergence of the stress tensor. Forces on atoms are calculated, and atoms are allowed to relax using a conjugate gradient technique until their residual forces have converged to less than 0.01 eV/Å. The Brillouin zone integration is performed using Monkhorst-Pack grids of $4 \times 6 \times 8$ during the iterations; but, to obtain higher quality state densities and to check the stability of the re-

sults, this number of k-points is increased to $6 \times 9 \times 12$ after convergence is reached.

2 Results and Discussion

In order to discuss the magnetic stability in a tiny range of energy, we start the structural relaxation from the experimental lattice parameters of $GdMnO_3$ (space group *Pnma*, a = 5.866Å, b = 7.431Å, and c = 5.318Å) [18]. we have optimized the internal structural parameters imposing AFM-A, AFM-C, AFM-G and AFM-E spin configuration on Mn d electrons in $GdMnO_3$ and the total energies with different concentration x are shown in Fig. 1. The AFM-E phase is most stable in $GdMnO_3$ ($x = 0$) at variance with experimental results reporting that the AFM-A phase is the spin ground state. The disagreement with experiments may again come from neglecting manybody effects within LDA/GGA and our results are consistent with previous calculated results [19]. The results also show that the AFM-E phase is more stable over the range of compositions x.

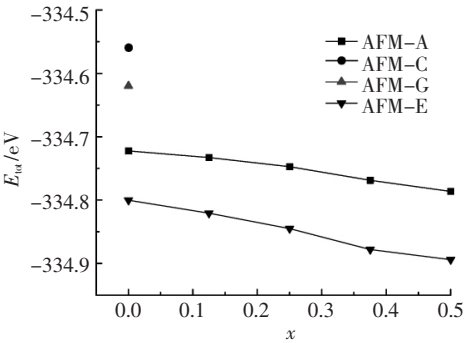

Fig.1 Total energy of AFM-A, AFM-C, AFM-G and AFM-E phases of GdMnO and total energy of AFM-A and AFM-E phases versus Ho concentration x

The lattice constants and the volume of the unit cell of AFM-A and AFM-E phases for different compositions are shown in Fig. 2. The errors of the lattice constants are about 1% in $GdMnO_3$, which are typical errors for GGA. For all concentrations we find that the single orthorhombic structure in $Gd_{1-x}Ho_xMnO_3$ can be maintained up to $x = 0.5$. On increasing Ho concentration, the lattice constants a, b and c are slightly decreasing continuously both in AFM-A and AFM-E phases. The effect of the doping on the structure is also seen from the the volume of the unit cell which almost linear decreasing is observed, indicating the lattice shrinking with increasing x. This variation is reasonable because of smaller Ho^{3+} ion than Gd^{3+} ion. The mean Mn-O bond distances and Mn − O − Mn angles in the ac plane are reported in Fig. 3. The Mn-O bond lengths l, m, s in $GdMnO_3$ are all slightly larger (<1%) than the experimental data [18] (l = 2.229Å, m = 1.944Å, and s = 1.915Å). The Mn-O bond length, l, m and s look rather constant over the compositions x. Because of the small size of the Gd ionic radius, $GdMnO_3$ shows a highly distorted perovskite structure with the Mn − O − Mn ac-plane angle $\phi \approx 146°$ [18]. The

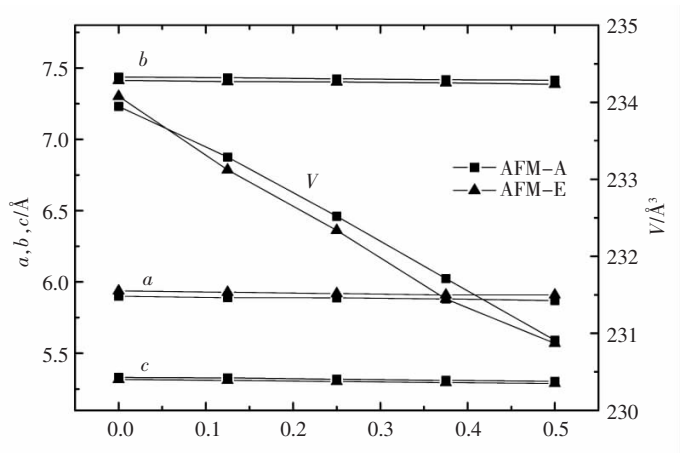

Fig.2 Lattice constants a, b, and c, volume of the unit cell in Gd Ho MnO versus Ho concentration x

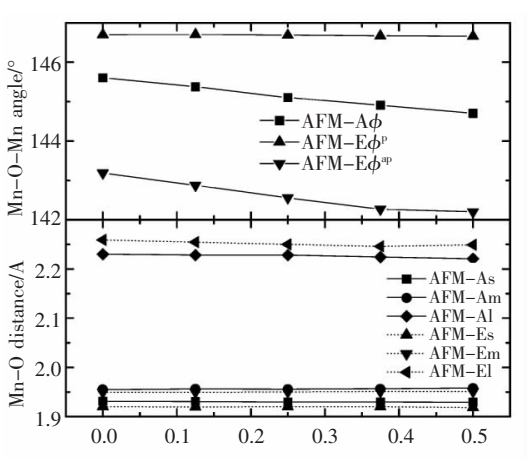

Fig.3 (upper panel) Mn-O bond distance of $Gd_{1-x}Ho_xMnO_3$ as a function of x. l,x: long and small Mn-O distances in ac plane, respectively; m:middle Mn-O distance along the b axis. The lines are plotted for an eye guide. (lower panel) Mn-O-Mn angles of $Gd_{1-x}Ho_xMnO_3$ as a function of x. φ: Mn-O-Mn angles in the ac plane; φ^p, φ^{ap}: Mn-O-Mn angles corresponding to the bonds with parrelel and antiparallel spins in the ac plane

lattice shrinking allows the reduction of the Mn – O – Mn angle ϕ in the AFM-A phase with increasing x (see Fig. 3), as well identified in earlier literature [20]. We also note that, in the AFM-E phase, the ϕ^{p} stays rather constant while the ϕ^{ap} decreases with x; the difference between ϕ^{p} and ϕ^{ap} which is at the basis of the polar atomic displacements [15] increases with the Ho doping. Recent experiment [15] shows that the doping leads to a transition of paraelectric phase into ferroelectric one, making $Gd_{1-x}Ho_xMnO_3$ multiferroic. The enhanced ferroelectric polarization originates from the reduction of Mn – O – Mn bond angle due to the Ho doping and the spin order of Ho spins at high doping level may also make contribution to the polarization which are not considered in our calculations.

We show the calculated total density of states (DOS) and various partial densities of states in $Gd_{1-x}Ho_xMnO_3$ in Fig. 4. The DOSs of spin-up and spin-down electrons are identical as expected for an AFM state. From the results, the band gap is estimated to be about 0.1 eV in AFM-A phase and 0.3 eV in AFM-E phase. However, it is well known that GGA greatly underestimates the band gap, especially for the 3d compounds. The real band gap might be much larger, confirming the experimental fact that $Gd_{1-x}Ho_xMnO_3$ is an insulator. For our discussion of the density of states, which is limited to an energy window of –8 eV to about 4 eV, we shall be primarily concern with the Mn d and O p states, since the Gd/Ho-derived states are quite small in the selected energy range. We see that the DOS near the Fermi level is mainly from Mn d and O p orbits and there is a strong hybridization between Mn d and O p states. In particular, the bands lying just below E_F and separated by the rest of the valence band are Mn-O bands (occupied hybridized e_g-like states (see Fig. 5)).

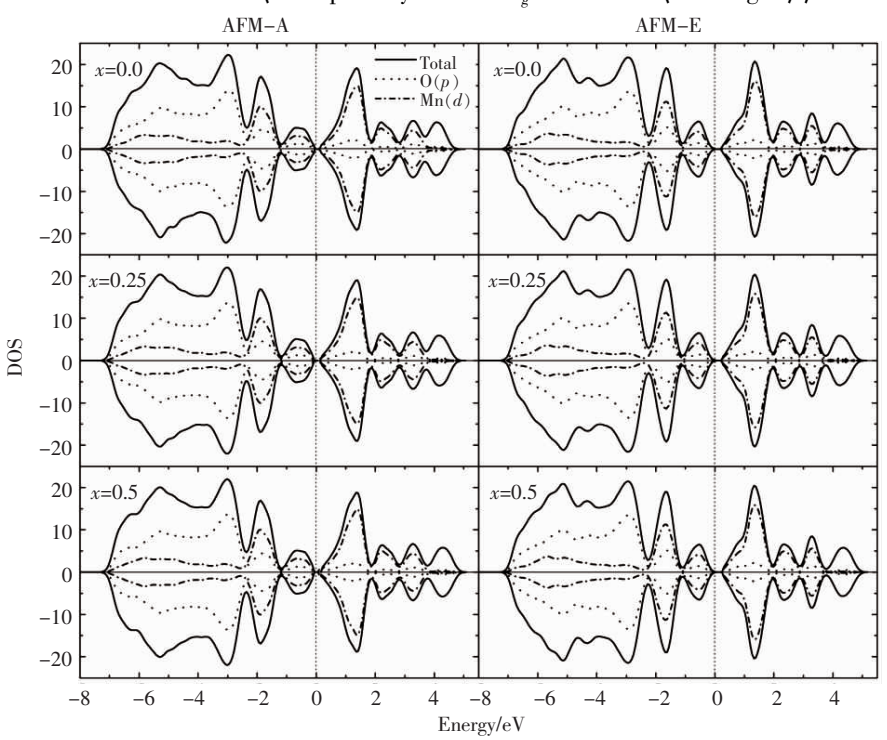

Fig.4 Total densities of states and partial densities of states of Mn *d*, and O *p* of AFM-A (left panel) and AFM-E (right panel) phases in $Gd_{1-x}Ho_xMnO_3$. The energy zero is taken at the Fermi level and the upper halves of each panel display the majority-spin states and the lower halves minority-spin states

Here, we would like to point out that the DOS does not change significantly both in AFM-A and AFM-E phases. We recall that the Mn d state is well localized and the character of the Mn-O bond is rather ionic in nature so it is not expected to undergo drastic changes as the bonding properties are concerned. In Fig. 5 we show the orbital-resolved densities of states of Mn and explain the calculation results in detail only for $x = 0.25$ in AFM-A and AFM-E phase. As expected, there exists a splitting between the valence t_{2g} and e_g states owing to the octahedral crystal-field effect. The John-Teller (JT) distortion and the tilting of the octahedra result in further

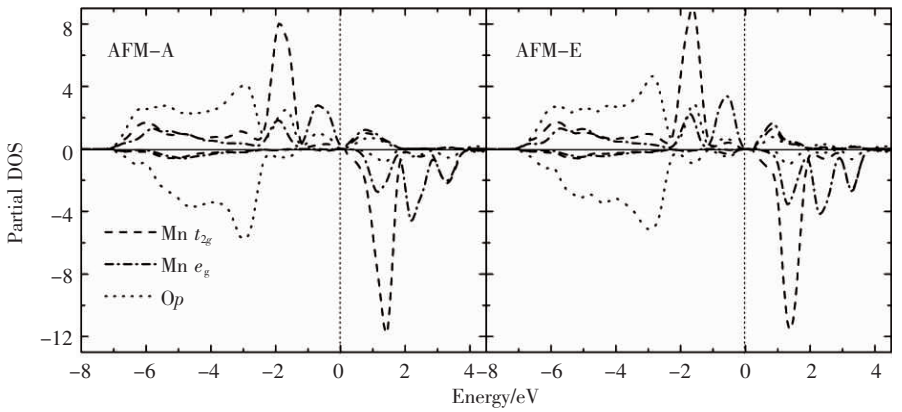

Fig.5 Orbital–resolved densities of states of Mn t_{2g} (red line) and e_g orbitals and the in *ac*–plane O 2*p* (navy line) orbital for $Gd_{1-x}Ho_xMnO_3$. The energy zero is taken at the Fermi level and the upper halves of each panel display the majority–spin states and the lower halves minority–spin states

splitting of e_g states. In the AFM–A phase, just below E_F is the Mn e_g state hybridized with the Op component; the lowest unoccupied band is dominated by the Mn e_g, Mn t_{2g} and O p states. In comparison with the AFM–A case, Fig. 5 clearly demonstrates that the hybridization of Mn e_g and O p in the *ac* plan is weaker in AFM–E phase which is due to the larger JT distortion.

The local magnetic moment of Mn is basically constant and equal to about 3.53 μ_B in AFM–A phase and 3.44 μ_B in AFM–E phase which is reduced with respect to the Hund's rule value 4 μ_B, reflecting the hybridization with O atoms. More information on the magnetic interactions between Mn atoms can be gained by considering a Heisenberg Hamiltonian and using this model to fit our calculated total energies (see Fig. 1). The difference between the total energy of AFM–A and AFM–E increases with x which indicates that the AFM–E spin configuration becomes more stable. This can be explained considering that, upon larger tilting, the overlap between Mn d and O p orbitals is not large enough to provide a strongly FM superexchange (SE) between Mn cations in the *ac* plane. This alters the delicate balance with the second–nearest–neighbor coupling SE interactions through Mn – O – O – Mn paths along the a direction. Upon significant distortions, the large second–nearest–neighbor coupling (of the order of few meV) AFM coupling prevails, therefore stabilizing the AFM–E ordering.

In order to better understand the trends of the magnetic properties, let us briefly discuss the local magnetic moment of the compounds in the AFM–E spin configuration. A general feature for the entire $Gd_{1-x}Ho_xMnO_3$ is that the oxygen atoms also possess small magnetic moments which originate from Mn d and O p hybridization in *ac* plan. The magnetic moments at O atoms range from ± 0.01 μ_B to ± 0.05 μ_B and the moments at O are directed parallel to the nearest–neighbor Mn atoms. These can also be observed in Fig. 6. The Mn atoms are ferromagnetically zigzag chains coupled and antiferromagnetically coupled to the neighboring chains, inducing the spin polarization of oxygen site significantly as seen in Fig. 6. The roughly spherical distributed spin densities of Mn indicate the nearly half-filled 3d orbitals. The spin density distribution from Fig.

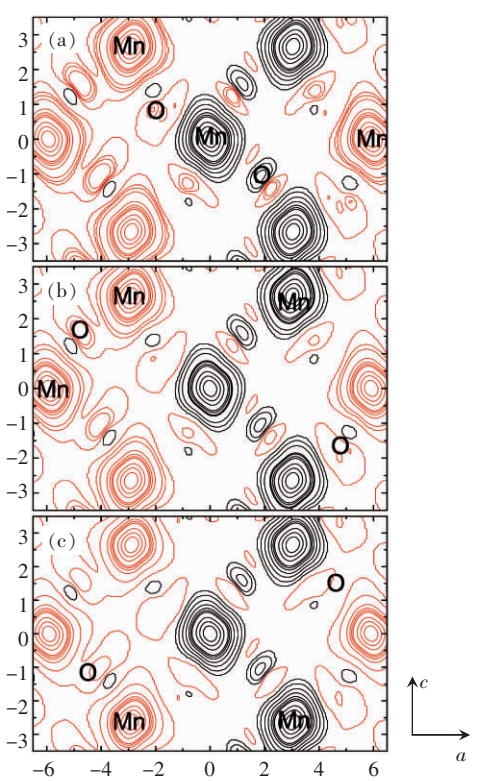

Fig.6 Contour plot of the spin density in the *ac* plane in $Gd_{1-x}Ho_xMnO_3$. (a) x=0, (b) x=0.25, and (c) x=0.5. Solid lines represent positive charge densities and dashed lines indicate negative charge density

6(a) to (c) also demonstrates that the overlap between Mn *d and O p* orbitals decreases with Ho concentration.

3 Conclusions

In conclusion, we have investigated a study of the structural, electronic, and magnetic properties of $Gd_{1-x}Ho_xMnO_3$ ($0.0 \leqslant x \leqslant 0.5$) using first-principles density functional theory within the generalized gradient approximation (GGA) schemes. The results show that the Mn-O bond length, *l*, *m* and *s* look rather constant over the compositions *x* and Mn – O – Mn bond angle decreases with *x* which originates the enhanced electric polarization in $Gd_{1-x}Ho_xMnO_3$. Our spin-polarized calculations give a insulating state for all *x* and the DOS does not change significantly both in AFM-A and AFM-E phases. The AFM-E spin configuration becomes more stable over the range of compositions *x* which can be explained considering that, upon larger tilting, the overlap between Mn *d* and O *p* orbitals is not large enough to provide a strongly FM superexchange (SE) between Mn cations in the *ac* plane.

[References]

[1] Eerenstein W, Mathur N D, Scott J F. Multiferroic and magnetoelectric materials [J]. Nature, 2006, 442: 759-765.

[2] Ramesh R, Spaldin N A. Multiferroics: progress and prospects in thin films [J]. Nat Mater, 2007, 6: 21-29.

[3] Hur N, Park S, Sharma P A, et al. Electric polarization reversal and memory in a multiferroic material induced by magnetic fields [J]. Nature, 2004, 429: 392-395.

[4] Kimura T, Goto T, Shintani H, et al. Magnetic control of ferroelectric polarization [J]. Nature, 2003, 426: 55-58.

[5] Goto T, Kimura T, Lawes G, et al. Ferroelectricity and giant magnetocapacitance in perovskite rare-earth manganites [J]. Phys Rev Lett, 2004, 92: 257 201(1-4).

[6] Tachibana M, Shimoyama T, Kawaji H, et al. Jahn-Teller distortion and magnetic transitions in perovskite $RMnO_3$ (R = Ho, Er, Tm, Yb, and Lu) [J]. Phys Rev B, 2007, 75: 144 425(1-5).

[7] Lorenz B, Wang Y Q, Chu C W. Ferroelectricity in perovskite $HoMnO_3$ and $YMnO_3$ [J]. Phys Rev B, 2007, 76: 104 405(1-3).

[8] Lin T H, Hsieh C C, Shih H C, et al. Anomalous magnetic ordering in b-axis-oriented orthorhombic $HoMnO_3$ thin films [J]. Appl Phys Lett, 2008, 92: 132 503(1-3).

[9] Hotta T, Moraghebi M, Feiguin A, et al. Unveiling new magnetic phases of undoped and doped manganites [J]. Phys Rev Lett, 2003, 90: 247 203(1-4).

[10] Salafranca J, Brey L. Phase diagram and incommensurate phases in undoped manganites [J]. Phys Rev B, 2006, 73: 024 422(1-9).

[11] Sergienko I A, Sen C, Dagotto E. Ferroelectricity in the magnetic E-phase of orthorhombic perovskites [J]. Phys Rev Lett, 2006, 97: 227 204(1-4).

[12] Picozzi S, Yamauchi K, Sanyal B, et al. Dual nature of improper ferroelectricity in a magnetoelectric multiferroic [J]. Phys Rev Lett, 2007, 99: 227 201(1-4).

[13] Kimura T, Lawes G, Goto T, et al. Magnetoelectric phase diagrams of orthorhombic $RMnO_3$ (R = Gd, Tb, and Dy) [J]. Phys Rev B, 2005, 71: 224 425(1-13).

[14] Goto T, Yamasaki Y, Watanabe H, et al. Anticorrelation between ferromagnetism and ferroelectricity in perovskite manganites [J]. Phys Rev B, 2005, 72: 220 403(R)(1-4).

[15] Zhang G Q, Luo S J, Dong S, et al. Enhanced ferroelectricity in orthorhombic manganites $Gd_{1-x}Ho_xMnO_3$ [J]. J Appl Phys, 2011, 109: 07D901(1-3).

[16] Perdew J P, Burke K, Ernzerhof M. Generalized gradient approximation made simple [J]. Phys Rev Lett, 1996, 77: 3 865-3 868.

[17] Kresse G, Furthmuller J. Efficient iterative schemes for ab initio total-energy calculations using a plane-wave basis set [J]. Phys Rev B, 1996, 54: 11 169-11 186.

[18] Mori T, Kamegashira N, Aoki K, et al. Crystal growth and crystal structures of the $LnMnO_3$ perovskites: Ln = Nd, Sm, Eu and Gd [J]. Mater Lett, 2002, 54: 238-243.

[19] Yamauchi K, Freimuth F, Stefan Blügel, et al. Magnetically induced ferroelectricity in orthorhombic manganites: microscopic origin and chemical trends [J]. Phys Rev B, 2008, 78: 014 403(1-10).

[20] Hemberger J, Schrettle F, Pimenov A, et al. Multiferroic phases of $Eu_{1-x}Y_xMnO_3$ [J]. Phys Rev B, 2007, 75: 035 118(1-8).

[责任编辑: 顾晓天]